INTERNATIONAL JOURNAL FOR NUMERICAL METHODS IN FLUIDS
Int. J. Numer. Meth. Fluids **29**: 899–920 (1999)

MULTIPHASE FLOW IN HETEROGENEOUS POROUS MEDIA: A CLASSICAL FINITE ELEMENT METHOD VERSUS AN IMPLICIT PRESSURE–EXPLICIT SATURATION-BASED MIXED FINITE ELEMENT–FINITE VOLUME APPROACH

R. HUBER AND R. HELMIG

Institut für Wasserbau, Universität Stuttgart, Pfaffenwaldring 61, 70550 Stuttgart, Germany

SUMMARY

Various discretization methods exist for the numerical simulation of multiphase flow in porous media. In this paper, two methods are introduced and analyzed—a full-upwind Galerkin method which belongs to the classical finite element methods, and a mixed-hybrid finite element method based on an implicit pressure–explicit saturation (IMPES) approach. Both methods are derived from the governing equations of two-phase flow. Their discretization concepts are compared in detail. Their efficiency is discussed using several examples. Copyright © 1999 John Wiley & Sons, Ltd.

KEY WORDS: multiphase flow; finite element method; mixed finite elements; heterogeneous porous media

1. INTRODUCTION

Multiphase flow processes are studied mainly in the context of enhanced oil recovery and environmental engineering. Although both fields deal with the same processes, reservoir simulation is generally done on much larger scales than subsurface remediation. Numerical simulators for multiphase flow in porous media were originally based on finite difference schemes, and were later based on finite volume and finite element methods. Various Petrov–Galerkin concepts were developed, e.g. the modified streamline Petrov–Galerkin method [1], or integrated finite difference methods [2], which accurately handle multiphase flow in homogeneous media. However, these methods are unable to capture flow phenomena occurring at heterogeneities, i.e. discontinuities in material properties such as absolute permeability, porosity, or of constitutive relationships. Full-upwind finite element methods, some of which can be interpreted as control-volume finite element methods [3], were introduced to deal with these problems. However, these methods generally introduce numerical dispersion.

In recent years a new discretization technique based on mixed finite elements has become popular in the field of petroleum reservoir simulation [4,5]. The advantage of these methods is that the primary variables and balance equations are in direct correspondence with the geometric discretization of the domain into elements and element edges. Hence, it is natural to formulate material properties with respect to elements and element interfaces. The discretization yields a sharp resolution of pressure and velocity fields. The mixed methods can be combined with a wide range of finite volume concepts based on an implicit pressure–explicit

CCC 0271–2091/99/080899–22$17.50

Received December 1996
Revised March 1997

saturation (IMPES) approach. 'IMPES' refers to a numerical concept in which pressure is implicitly formulated, and saturation explicitly formulated.

Mixed methods for two-phase flow in porous media have been discussed by Chavent and Jaffre [4] and Durlofsky [6]. However, they have not been developed in the context of multiphase flow processes with classical finite element methods. Durlofsky [7] compared mixed and control volume finite element approximations for the Darcy velocity field of single-phase flow and found that the mixed finite element method clearly gave, in the case of highly heterogeneous media, more physically realistic streamlines than the Galerkin- type methods.

The goal of this paper is to compare the two quite different approaches of classical finite elements and mixed finite elements with regard to their ability to simulate multiphase flow processes, showing the advantages and the limitations inherent in each approach. Representative methods of each class, the full-upwind Galerkin [8] and an IMPES-based mixed-hybrid finite element method [9] are presented, their conceptions and discretizations are compared, and their performance is demonstrated in several examples.

First, in Section 2, the governing equations are introduced and the numerical schemes of the two methods are developed. In Section 3, a comparison of the discretization concepts is undertaken. Then in Section 4, the different aspects are illustrated by numerical examples. The problems presented are one- and two-dimensional without any capillary effects. Finally, in Section 5 conclusions are summarized, and current and future developments for the simulation of multiphase flow processes are mentioned.

2. GOVERNING EQUATIONS AND NUMERICAL DISCRETIZATION

Flow of two (or more) immiscible fluids in porous media is described by Darcy's law and the continuity equation for each fluid. The Darcy velocity for phase α is given by

$$v_\alpha = -\lambda_\alpha \boldsymbol{K}(\nabla p_\alpha - \varrho_\alpha g), \quad \alpha \in \{\mathrm{w}, \mathrm{n}\}, \tag{1}$$

where p_α is the phase pressure, $k_{\mathrm{r}\alpha}$ the relative permeability, μ_α the viscosity of phase ϱ_α, the density, $\boldsymbol{K}$ the absolute permeability tensor, and g the gravitational acceleration vector. Subscripts w and n denote the wetting phase and the non-wetting phase, respectively. Mobility $\lambda_\alpha = k_{\mathrm{r}\alpha}/\mu_\alpha$ of each phase α is defined as the ratio of the relative permeability $k_{\mathrm{r}\alpha}$ to the fluid viscosity μ_α.

The continuity equation for two-phase flow in porous media is given by

$$\frac{\partial(\varrho_\alpha \phi S_\alpha)}{\partial t} = -\nabla \cdot [\varrho_\alpha v_\alpha] + \varrho_\alpha q_\alpha, \quad \alpha \in \{\mathrm{w}, \mathrm{n}\}, \tag{2}$$

where S_α is the saturation and q_α represents the volumetric source–sink rate of phase α.

In addition to Equations (1) and (2), the following relationships must also be satisfied:

$$p_\mathrm{c} = p_\mathrm{n} - p_\mathrm{w} \tag{3}$$

$$S_\mathrm{w} + S_\mathrm{n} = 1. \tag{4}$$

The relative permeabilities $k_{\mathrm{r}\alpha}(S_\alpha)$, $\alpha \in \{\mathrm{w}, \mathrm{n}\}$, as well as capillary pressure $p_\mathrm{c}(S_\mathrm{w})$ are unique functions of the saturation. It should be noted that these constitutive relationships are strongly non-linear functions.

We have restricted our investigation to incompressible fluid flow, i.e. constant densities ϱ_n and ϱ_w. Furthermore, we assume a constant porosity over the entire domain. Under these assumptions, the continuity equation is reduced to

$$\phi \frac{\partial S_\alpha}{\partial t} = -\nabla \cdot v_\alpha + q_\alpha, \quad \alpha \in \{\mathrm{w}, \mathrm{n}\}. \tag{5}$$

2.1. Full-upwind Galerkin method

Darcy's law (1) for fluid flow in porous media and the continuity equation (5) form the basis for the description of (incompressible) multiphase flow processes. Pressure and saturation of each phase can be coupled using constraints (3) and (4). Substituting (1), (3) and (4) into (5) yields the coupled pressure–saturation equations for incompressible two-phase flow with unknowns p_w and S_n:

$$\begin{aligned} -\phi \frac{\partial S_\mathrm{n}}{\partial t} &= \nabla \cdot [\lambda_\mathrm{w} \boldsymbol{K}(\nabla p_\mathrm{w} - \varrho_\mathrm{w} g)] + q_\mathrm{w} \\ \phi \frac{\partial S_\mathrm{n}}{\partial t} &= \nabla \cdot [\lambda_\mathrm{n} \boldsymbol{K}(\nabla p_\mathrm{w} + \nabla p_\mathrm{c} - \varrho_\mathrm{n} g)] + q_\mathrm{n}. \end{aligned} \tag{6}$$

These equations form the basis for a number of Galerkin finite element methods. When compressibility is taken into account in these equations, they are extremely general in their applicability. They include the effects of capillary pressure and relative permeability, as well as variations of the absolute permeability and the porosity with position. The differential equations are discretized using the lowest order, conforming the Galerkin finite element method. Standard Galerkin methods have the same shape and test space. A generalization of their approach represents the Petrov–Galerkin methods which use distinct spaces for test and shape functions. In contrast to many Petrov–Galerkin approaches which do partial upwinding, the full-upwind Galerkin approach uses the test functions from the standard Galerkin method in conjunction with the upstream mobilities.

The system of Equation (6) can be classified as a mixed hyperbolic–parabolic type. The system describing one-dimensional two-phase flow with incompressible fluids and no capillary pressure is reduced to the well-known Buckley–Leverett equation. This equation is a non-linear hyperbolic equation with respect to the fluid saturation. On the other hand, if the entire domain is single phase, then the system of equations reduces to a parabolic equation with respect to the fluid pressure. Therefore, we regard pressure as a 'parabolic-type' and saturation as a 'hyperbolic-type' variable [10].

The unknown quantities—pressures and saturations—are approximated by standard finite elements. Hence they can be expressed by following linear combinations:

$$\tilde{p}_\mathrm{w} = \sum_{i \in I} \hat{p}_{\mathrm{w},i} N_i \qquad \tilde{p}_\mathrm{c} = \sum_{i \in I} \hat{p}_{\mathrm{c},i} N_i \qquad \tilde{S}_\mathrm{n} = \sum_{i \in I} \hat{S}_{\mathrm{n},i} N_i, \tag{7}$$

where N_i are the base functions of the corresponding approximation space with the property $N_i = \delta_{ij}$ at node j, δ is the Kronecker delta, and the hat values are the values of approximation at the corresponding nodes. I is the set of all nodes of the discretization of domain Ω, and η_i is the set of all neighbouring nodes of node i, i.e. all nodes that have an element with i in common.

Test space and approximation space are the same for the full-upwind Galerkin method. However, a form of upwinding is introduced by the evaluation of mobilities at upstream nodes. In the two-dimensional case, the upwinding for quadrilateral elements is controled by the gradients φ_α (see Equation (11)) evaluated at edge mid-points [8]. In order to improve the stability of the method, mass lumping is applied to the mass matrix. In addition, for Equation (5), which is semi-discretized in time, a fully implicit formulation is chosen. This gives the following functional equations:

$$G_\alpha(\hat{p}_\mathrm{w}^{n+1}, S_\mathrm{n}^{n+1}) := (-1)^{\delta_{\alpha n}} \frac{\phi M_{ii}^{\mathrm{lump}}}{\Delta t}(\hat{S}_{\mathrm{n},i}^{n+1} - \hat{S}_{\mathrm{n},i}^{n}) + \sum_{j\in\eta_i} \lambda_{\alpha,ij}^{\mathrm{up},n+1}\varphi_{\alpha,ij}^{n+1}\gamma_{ij} + \int_\Omega q_\alpha^{n+1} N_i \,\mathrm{d}\Omega + m_{\alpha,i}^{n+1} = 0, \quad \alpha\in\{\mathrm{w}, \mathrm{n}\}, \tag{8}$$

where M_{ij}^{lump} is the lumped mass matrix defined by

$$M_{ij}^{\mathrm{lump}} = \delta_{ij}\sum_{j\in I}\int_\Omega N_i N_j \,\mathrm{d}\Omega = \delta_{ij}\int_\Omega N_i \mathrm{d}\Omega, \tag{9}$$

and the upstream mobilities $\lambda_{\alpha,ij}^{\mathrm{up}}$ are taken as

$$\lambda_{\alpha,ij}^{\mathrm{up}} = \begin{cases} \lambda_{\alpha,i}\colon \gamma_{ij}\varphi_{\alpha,ij} \le 0 \\ \lambda_{\alpha,j}\colon \gamma_{ij}\varphi_{\alpha,ij} > 0 \end{cases}, \quad \alpha\in\{\mathrm{w}, \mathrm{n}\}. \tag{10}$$

Gradient $\varphi_{\alpha,ij}$ which comprises phase pressure gradient as well as gravity is given by

$$\varphi_{\alpha,ij}^{n+1} = (\hat{p}_{\mathrm{w},j}^{n+1} - \hat{p}_{\mathrm{w},i}^{n+1}) + \delta_{\alpha n}(\hat{p}_{\mathrm{c},j}^{n+1} - \hat{p}_{\mathrm{c},i}^{n+1}) - \varrho_\alpha g(\hat{D}_j - \hat{D}_i), \tag{11}$$

where $\hat{D}_i$ is the depth at node i with respect to a reference point, and g, the gravitational constant. The transmissivity integral γ_{ij} is expressed by

$$\gamma_{ij} = -\int_\Omega \nabla N_i \boldsymbol{K} \nabla N_j \,\mathrm{d}\Omega. \tag{12}$$

γ_{ij} is negative in the one-dimensional case and for square elements in two dimensions. The Neumann boundary term $m_{\alpha,i}$ for phase α at boundary node i is given by

$$m_{\alpha,i} = \int_{\Gamma_\alpha \mathrm{N}} N_i \lambda_\mathrm{w} \boldsymbol{K}(\nabla p_\mathrm{w} + \delta_{\alpha n}\nabla p_\mathrm{c} - \varrho_\alpha g)\cdot \vec{n}_\Gamma \,\mathrm{d}\Gamma, \tag{13}$$

where $\vec{n}_\Gamma$ is the outward unit normal to boundary Γ.

A Newton–Raphson iterative scheme is utilized to solve the system of functional Equation (8) for vector $(\hat{p}_\mathrm{w}^{n+1}, \hat{S}_\mathrm{n}^{n+1})$, which has the node values of $\tilde{p}_\mathrm{w}$ and $\tilde{S}_\mathrm{n}$ as components. The corresponding linear system of equations is the product of the Jacobian of $(G_\mathrm{w}, G_\mathrm{n})$ times the correction vector $(\Delta\hat{p}_\mathrm{w}, \Delta\hat{S}_\mathrm{n})$ on the left-hand side and $(G_\mathrm{w}, G_\mathrm{n})$ on the right-hand side [1,11]. The Jacobian and the right-hand side vector are evaluated with the result of the last iteration. The iteration process is continued until the correction vector satisfies a specified condition.

2.2. Mixed finite element–finite volume approach

2.2.1. Differential equations. Pressure and saturation are decoupled in the mixed finite element–finite volume (FE–FV) approach. Two differential equations, a pressure and a saturation equation, which have pressure and saturation as primary variables, respectively, can be derived from the basis Equations (1), (3)–(5).

To derive the pressure equation, one must eliminate the time derivatives of the saturations in the continuity equation (5) using constraint (4). This is achieved by adding the two continuity equations. This gives us the following equation:

$$-\nabla\cdot[v_\mathrm{n} + v_\mathrm{w}] + q_\mathrm{t} = 0, \tag{14}$$

where $q_\mathrm{t} = q_\mathrm{n} + q_\mathrm{w}$ is the total volumetric flow rate into the domain.

By introducing an average pressure $p_\mathrm{avg} = (p_\mathrm{n} + p_\mathrm{w})/2$ of the two-phase system, the phase pressures p_n and p_w can be expressed in terms of average pressure p_avg and capillary pressure p_c (see Equation (3)) in the following way:

$$p_n = p_{avg} = \frac{1}{2} p_c, \qquad p_w = p_{avg} - \frac{1}{2} p_c. \tag{15}$$

Substitution of Equations (1) and (15) into (14) yields the pressure equation:

$$\nabla \cdot [\lambda_t \boldsymbol{K} \nabla p_{avg}] + \frac{1}{2} \nabla \cdot [(\lambda_n - \lambda_w) \boldsymbol{K} \nabla p_c] - \nabla \cdot [(\varrho_n \lambda_n + \varrho_w \lambda_w) \boldsymbol{K} g] + q_t = 0, \tag{16}$$

where $\lambda_t = \lambda_n + \lambda_w$ is the total mobility of the system.

In the case of reservoir simulation problems, capillary pressure is generally small compared with the average pressure. Therefore, capillary pressure terms were neglected in the following investigations. The gravitational terms are also neglected in the following, resulting in a simplified form of the pressure equation which is given by

$$\nabla \cdot [\lambda_t \boldsymbol{K} \nabla p_{avg}] + q_t = 0. \tag{17}$$

The resulting differential equation represents an elliptic equation [12]. If we also assume that there are no sources and sinks inside of the domain, the pressure equation can be expressed by the following system of equations:

$$v_t = \lambda_t \boldsymbol{K} \nabla p_{avg} \tag{18}$$

$$\nabla \cdot v_t = 0, \tag{19}$$

where $v_t = v_n + v_w$ is the total velocity of the two-phase system. These two equations form the basis equations of the mixed finite element formulation (in Section 2.2.3).

In order to derive the saturation equation, the differential equation must be formulated in terms of a specific phase saturation. Here, the saturation equation is written in terms of the wetting phase saturation. From Equations (1) and (3), the following equality can be derived:

$$\lambda_n \lambda_w \boldsymbol{K} \nabla p_c = \lambda_n v_w - \lambda_w v_n + \lambda_n \lambda_w (\varrho_n - \varrho_w) \boldsymbol{K} g. \tag{20}$$

Equation (20) can be modified in order to get

$$\lambda_t v_w = \lambda_w v_t + \lambda_n \lambda_w \boldsymbol{K} (\nabla p_c (\varrho_w - \varrho_n) g). \tag{21}$$

With the fractional flow function $f_w = \lambda_w / \lambda_t$ and the dimensionless expression

$$G_d = \frac{(\varrho_w - \varrho_n) \boldsymbol{K} g}{\mu_n v_t}, \tag{22}$$

which represents the ratio of gravitational to convective effects, Equation (21) can be expressed in a more compact form:

$$v_w = v_t f_w (1 - k_{rn} G_d) - \lambda_n f_w \boldsymbol{K} \nabla p_c. \tag{23}$$

Substitution of Equation (23) into (5) for the wetting phase yields the saturation equation:

$$\phi \frac{\partial S_w}{\partial t} = -\nabla \cdot [v_t f_w (1 - k_{rn} G_d)] - \nabla \cdot [\lambda_n f_w \boldsymbol{K} \nabla p_c] + q_w. \tag{24}$$

When we assume that there are no sources or sinks inside the domain, i.e. $q_w = q_t = 0$, and omit the gravitational term, the following equation is obtained:

$$\phi \frac{\partial S_w}{\partial t} = -\nabla \cdot [v_t f_w] - \nabla \cdot [\lambda_n f_w \boldsymbol{K} \nabla p_c]. \tag{25}$$

The first divergence term can be expanded by

$$\nabla\cdot[v_t f_w] = f_w \underbrace{\nabla\cdot v_t}_{=0} + v_t \nabla f_w = v_t \frac{df_w}{dS_w}\nabla S_w. \tag{26}$$

$\nabla\cdot v_t$ is zero since we have assumed a source- and sink-free domain. Defining function h_w by

$$h_w = -\lambda_n f_w \boldsymbol{K} \frac{dp_c}{dS_w}, \tag{27}$$

yields a very simple form of the saturation equation:

$$\phi \frac{\partial S_w}{\partial t} = -v_t \frac{df_w}{dS_w}\nabla S_w + \nabla\cdot[h_w \nabla S_w]. \tag{28}$$

It should be noted that when the second term on the right-hand side is dominant, i.e. capillary pressure effects play a major role and h_w becomes large, the saturation equation becomes strongly parabolic. However, when capillary pressure effects are negligible or absent, the saturation equation reduces to a first-order non-linear hyperbolic differential equation.

2.2.2. Structure of the implicit-pressure–explicit saturation concept. In contrast to simultaneous approximation of pressure and saturation by the iterative scheme of the full-upwind Galerkin method, the IMPES concept involves the sequential solution of the pressure equation and the saturation equation (see Figure 1). The presented IMPES concept is based on these two equations. The two differential equations depend only on the pressures and the saturations of the two-phase system. While the pressure equation is partially or fully implicitly formulated, the explicit form of the saturation equation is used. In general, the fully implicit form of the pressure equation is used. The pressure equation is discretized by a mixed finite element formulation which is hybridized to obtain a linear system of equations with favourable properties. The edge mobilities to be used by the mixed-hybrid method are derived from the

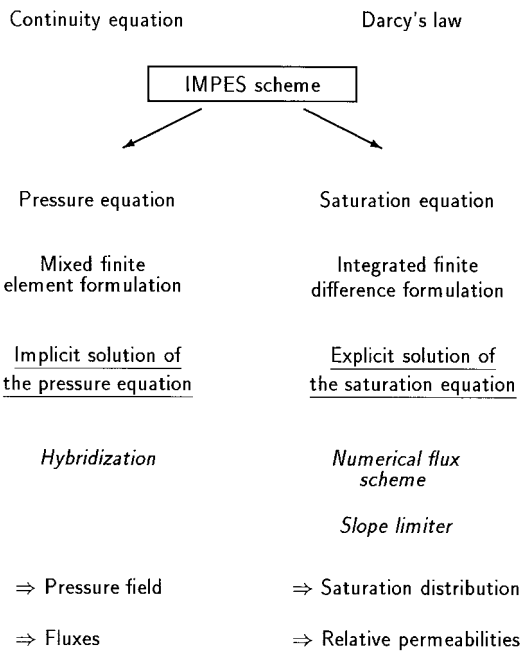

Figure 1. Structure of the presented IMPES method.

corresponding upstream saturations of the preceeding time step. The pressure field and the fluxes over the element edges of the partition are obtained and used in the saturation equation which is formulated explicitly by an integrated finite difference approach. Then, the element saturations are determined using a slope limiter technique based on the EO (Engquist–Osher) numerical flux scheme [13]. It is important to note that the decoupling of the solution for pressure and saturation is only justified when the interaction between these two quantities is relatively small.

2.2.3. Mixed-hybrid finite element method. A mixed-hybrid method is applied to the pressure equation. The pressure equation can be split into two equations, (18) and (19). The notion of mixed finite element methods entails the weighting of a system of functional equations by distinct test spaces. The corresponding integral equations for (18) are weighted by test functions from $H(\mathrm{div};\Omega)$, and the ones corresponding to (19) are weighted by $L^2(\Omega)$-functions.

$H(\mathrm{div};\Omega)$ is defined by

$$H(\mathrm{div};\Omega)=\{u\in(L^2(\Omega))^2 \,|\, \nabla\cdot u\in L^2(\Omega)\}. \tag{29}$$

Because these spaces are of infinite dimension, we approximate them by finite dimensional function spaces $\tilde{\tilde{X}}(\Omega)$ and $Y(\Omega)$. These spaces are closely related to the discretization of the domain, i.e. the partitioning $\mathscr{T}_h$ of the domain into elements $K\in\mathscr{T}_h$ and edges $e_i\in\varepsilon_h$, where ε_h denotes the set of all element edges.

$\tilde{\tilde{X}}(\Omega)$ and $Y(\Omega)$ are defined by

$$\tilde{\tilde{X}}(\Omega)=\{u\in H(\mathrm{div};\Omega) \,|\, u_{|K}\in \mathrm{RT}_0(K) \quad \forall K\in\mathscr{T}_h\}=\{u\in\tilde{X}(\Omega) \,|\, u\cdot\vec{n}_{\partial K}+u\cdot\vec{n}_{\partial K'}=0 \text{ along } e_i=\partial K\cap\partial K' \quad \forall e_i\varepsilon_h\} \tag{30}$$

$$Y(\Omega)=\nabla\cdot\tilde{\tilde{X}}(\Omega)=\{q\in L^2(\Omega) \,|\, q_{|K}\in Y_K \quad \forall K\in\mathscr{T}_h\}, \tag{31}$$

where

$$\tilde{X}(\Omega)=\{v\in(L^2(\Omega))^2 \,|\, v_{|K}\in \mathrm{RT}_0(K) \quad \forall K\in\mathscr{T}_h\}, \tag{32}$$

and $Y_K=\nabla\mathrm{RT}_0(K)=\{y_K \,|\, y_K=\text{const. in } K\}$. $\mathrm{RT}_0(K)$ is the lowest order Raviart–Thomas space for element K [14,15].

We assume that the permeability tensor $\boldsymbol{K}$ is invertible. Then Equation (18) can be multiplied by $\boldsymbol{K}^{-1}$ and divided by λ_t. The resulting equation is

$$\frac{1}{\lambda_t}\boldsymbol{K}^{-1}v_t=\nabla p_{\mathrm{avg}}. \tag{33}$$

The weak formulation of (18) and (19) with test functions from the function spaces $\tilde{\tilde{X}}(\Omega)$ and $\mathrm{Y}(\Omega)$, respectively, represents their mixed finite element formulation. The velocity field v_t is discretized by function $\tilde{v}_h\in\tilde{\tilde{X}}(\Omega)$ and the pressure field p_{avg} by $\tilde{p}_h\in Y(\Omega)$. Then the variational equations are given by the following:

Find $(\tilde{v}_h,\tilde{p}_h)\in\tilde{\tilde{X}}(\Omega)\times Y(\Omega)$ such that

$$\int_\Omega \frac{1}{\lambda_t}\boldsymbol{K}^{-1}\tilde{v}_h\cdot u\,\mathrm{d}\Omega-\int_\Omega \tilde{p}_h\nabla\cdot u\,\mathrm{d}\Omega=\int_{\Gamma_D}\tilde{p}_{\mathrm{Dh}}u\cdot\vec{n}_\Gamma\,\mathrm{d}\Gamma \quad \forall u\in\{u\in\tilde{\tilde{X}}(\Omega) \,|\, u\cdot\vec{n}_{\Gamma\mathrm{N}}=0\}$$

$$\int_\Omega \nabla\cdot\tilde{v}_h q\,\mathrm{d}\Omega=0 \quad \forall q\in Y(\Omega) \qquad \int_{e_i}\tilde{v}_h\cdot\vec{n}_\Gamma\,\mathrm{d}\Gamma=\tilde{Q}_{\mathrm{N},e_i} \quad \forall e_i\subset\Gamma_{\mathrm{N}}. \tag{34}$$

$\tilde{Q}_{\mathrm{N},e_i}$ is the volumetric flow rate over element edge e_i of the Neumann boundary and $\tilde{p}_{\mathrm{Dh}}$ is the discretized representation of the pressure along the Dirichlet boundary.

The mixed-hybrid finite element method is based on dualization principles. For this reason, an additional function space $Z(\Omega)$ for the Lagrange multipliers $\mathscr{T} P_{e_i}$ is needed. It is defined by

$$Z(\Omega) = \{z | z_{e_i} = \text{constant} \quad \forall e_i \in \varepsilon_h\}. \tag{35}$$

Moreover, $\tilde{X}(\Omega)$—a more general space than $\tilde{\tilde{X}}(\Omega)$—is necessary. $\tilde{X}(\Omega)$ has already been defined by Equation (32).

The variational equations of the mixed-hybrid finite element method have the form:

Find $(v_h, p_h, t_{p_h}) \in \tilde{X}(\Omega) \times Y(\Omega) \times Z(\Omega)$ such that

$$\int_\Omega \frac{1}{\lambda_t} \boldsymbol{K}^{-1} v_h \cdot u \, \mathrm{d}\Omega - \int_\Omega p_h \nabla \cdot u \, \mathrm{d}\Omega + \sum_{e_i \in \varepsilon_h} \sum_{K \in \mathscr{T}_h, \partial K \supset e_i} \int_{e_i} t_{p_h} u \cdot \vec{n}_{\partial K} \, \mathrm{d}e_i = 0 \quad \forall u \in \tilde{X}(\Omega) \tag{36}$$

$$\int_\Omega \nabla \cdot v_h q \, \mathrm{d}\Omega = 0 \quad \forall q \in Y(\Omega) \tag{37}$$

$$\sum_{e_i \in \varepsilon_h} \sum_{K \in \mathscr{T}_h, \partial K \supset e_i} \int_{e_i} v_h \cdot \vec{n}_{\partial K} z \, \mathrm{d}e_i = \int_{\Gamma_N} q_{Nh} \cdot \tilde{n}_\Gamma z \, \mathrm{d}\Gamma \quad \forall z \in \{z \in Z(\Omega) | z_{|\Gamma_D} = 0\} \tag{38}$$

$$t_{p_h} = t_{p\mathrm{Dh}} \text{ along } \Gamma_D. \tag{39}$$

The natural choice for basis functions of the finite dimensional function spaces $\tilde{X}(\Omega)$ and $Y(\Omega)$ is

$$u_{K,i} \in \tilde{X}(\Omega) \begin{cases} u_{K,i|_{K'}} = 0 & \forall K' \in \mathscr{T}_h, \quad K' \neq K \\ \left| \int_{e_i} \nabla \cdot u_{K,i} \, \mathrm{d}e_j = \delta_{ij} \right. & \forall e_j \in \varepsilon_h, \quad e_j \subset \partial K \end{cases} \tag{40}$$

$$\chi_K \in Y(\Omega) \quad \chi_{K|K'} = \delta_{KK'} \quad \forall K, K' \in \mathscr{T}_h. \tag{41}$$

This yields the following representation of the approximated velocity and pressure field:

$$v_{h|K} = \sum_{j=1}^{n_K} Q_{K,e_j} u_{K_j} \tag{42}$$

$$p_{h|K} = P_K \tag{43}$$

$$p_{h|e_i} = TP_{e_i} \tag{44}$$

n_K denotes the number of edges of element K. Equation (42) states that the velocity field v_h inside of each element K is completely determined by the element edge fluxes Q_{K,e_j}. The discretized pressure field is given by element values P_K and element edge values TPe_i. Figure 2 illustrates the discretized pressure field, velocity field, and saturation distribution.

The discretized form of variational Equations (36)–(39) is then

$$\begin{aligned} &\sum_{j=1}^{n_K} Q_{K,e_j} \int_K \frac{1}{\lambda_t} \boldsymbol{K}^{-1} u_{K,j} \cdot u_{K,i} \, \mathrm{d}K \\ &\quad = P_K \underbrace{\int_K \nabla \cdot u_{K,i} \, \mathrm{d}K}_{=1} - \sum_{j=1}^{n_K} TP_{e_j} \underbrace{\int_{e_j} u_{K,i} \cdot \vec{n}_{\partial K} \, \mathrm{d}e_j}_{=\delta_{ij}} \\ &\quad i = 1, \ldots, n_K \; \forall K \in \mathscr{T}_h \end{aligned} \tag{45}$$

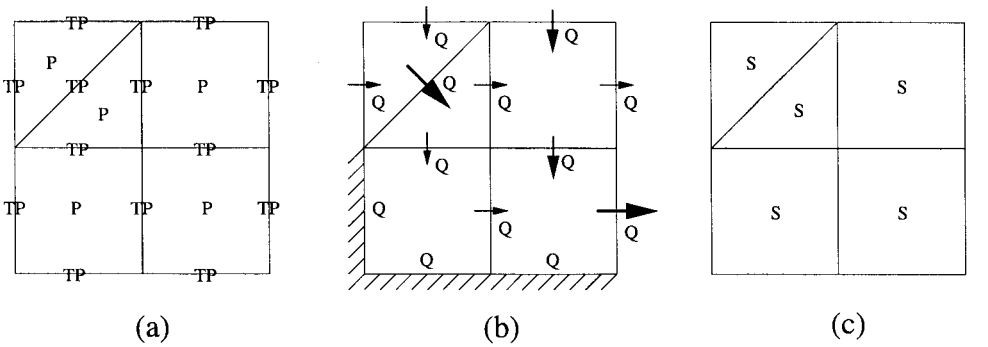

Figure 2. Discretization of the mixed-hybrid finite element method: (a) pressure field (element pressures P, edges TP); (b) velocity field (edge fluxes Q); (c) saturation distribution (element saturations S).

$$\sum_{j=1}^{n_K} Q_{K,e_j} \underbrace{\int_K \nabla \cdot u_{K,i} \, \mathrm{d}K}_{=1} = 0 \quad \forall K \in \mathcal{T}_h \tag{46}$$

$$Q_{K,e_j} + Q_{K',e_j} = 0 \quad \forall e_j = \partial K \cap \partial K' \tag{47}$$

$$Q_{K,e_i} = Q_{\mathrm{N},e_i} \quad \forall e_i \subset \Gamma_{\mathrm{N}} \tag{48}$$

$$TP_{e_i} = TP_{D,e_i} \quad \forall e_i \subset \Gamma_D. \tag{49}$$

The dualization principle is applied to the incompressibility condition (46) and the continuity of fluxes across element edges (47). This means the Q_{K,e_j} expressions in (45) are isolated and substituted into (46), giving the discretized element balance equations. The P_K terms are extracted in the element balance equations and substituted into the equations which emerge from the substitution of the Q_{K,e_j}'s of (46) into (47) and (48). By these substitutions, element pressures P_K and edge fluxes Q_{K,e_j} are eliminated. The resulting mixed-hybrid system of equations has only the Lagrange multipliers TP_{e_i}, which represent the edge pressures, as primary variables. It can be shown that the corresponding system matrix is positive definite and consequently the system can easily be solved, for instance, with a conjugate gradient method [4,9]. Afterwards, the gained $TP_{e_i}^{n+1}$ values can be used to obtain the element pressure values P_K. Finally, all pressure values are needed to solve Equation (45) for the element edge fluxes Q_{K,e_j}.

2.2.4. Finite volume method. After application of the mixed-hybrid FE method, the pressure field at the new time level is known. Moreover, the total flux across each element edge of the partition during the current time step is also known. Now the phase saturations at the new time level can be computed. A finite volume method is applied to the saturation equation. The method corresponds to the finite element concept with test functions χ_K, which are piecewise constant. The weak formulation of the differential equation is represented by the integrals over each element. Therefore, this method is also called an integrated finite difference scheme. Consequently, the weak formulation of the saturation equation reads

$$\int_\Omega \phi \frac{\partial S_{\mathrm{w}}}{\partial t} \chi_K \, \mathrm{d}\Omega = -\int_\Omega \nabla \cdot [v_{\mathrm{t}} f_{\mathrm{w}} (1 - k_{\mathrm{rn}} G_d)] \chi_K \, \mathrm{d}\Omega - \int_\Omega \nabla \cdot [\lambda_{\mathrm{n}} f_{\mathrm{w}} \boldsymbol{K} \nabla p_{\mathrm{c}}] \chi_K \, \mathrm{d}\Omega + \int_\Omega q_{\mathrm{w}} \chi_K \, \mathrm{d}\Omega, \tag{50}$$

where the test functions χ_K are characteristic functions with respect to partition $\mathcal{T}_h$ of the domain, i.e.

$$\chi_K = \begin{cases} 1 & \text{in element } K \\ 0 & \text{else} \end{cases}. \tag{51}$$

The discretized equation for each element K with element saturation S_K, fluxes Q_{K,e_i} and a backward Euler time discretization applied to the time derivative is

$$\phi |K| \frac{S_K^{n+1} - S_K^n}{\Delta t} = - \sum_{e_i:\text{edges of } K} f_w (1 - k_{rn} G_d) Q_{K,e_i} - \sum_{e_i:\text{edges of } K} \int_{e_i} \lambda_n f_w \boldsymbol{K} \nabla p_c \cdot \vec{n}_{e_i} \, de_i + q_w |K|, \tag{52}$$

where $|K|$ is the volume of element K.

The saturation S_K^{n+1} in element K at the new time level $n+1$ is determined by

$$S_K^{n+1} = S_K^n + \Delta t (\mathscr{F}_{\text{konv/grav}}^{n+1} + \mathscr{F}_{\text{diff}}^{n+1}), \tag{53}$$

where the convective–gravitative and diffusive components of the flux are treated separately. They are given by

$$\mathscr{F}_{\text{konv/grav}}^{n+1} = - \frac{1}{\phi |K|} \sum_{i=1}^{n_K} f_w Q_{e_i}^{n+1} (1 - G_d) \tag{54}$$

$$\mathscr{F}_{\text{diff}}^{n+1} = \frac{1}{\phi |K|} \sum_{i=1}^{n_K} \int_{e_i} \lambda_n f_w \boldsymbol{K} \nabla p_c \cdot \vec{n}_{e_i} \, de_i. \tag{55}$$

Chavent and Jaffre [4] give two ways to determine the capillary pressure dependent fluxes. They solve a linear system of equations which can be formulated, either with respect to edges and element mid-points, or only for edges. If convection is dominant, it is not necessary to calculate the diffusive fluxes with higher accuracy than the convective ones. Thus, it is sufficient to choose the second variant. Furthermore, this variant saves much computation time, especially in two or more dimensions. To approximate the fluxes, Durlofsky [6] proposed another approach based on an essentially non-oscillatory (ENO) Runge–Kutta scheme [16].

The Buckley–Leverett problem [17] shows that discontinuities in the saturation distribution, e.g. shocks, can occur. Therefore the method applied to such problems should meet several requirements. It should give high resolutions of saturation fronts without producing spurious oscillations. This means that the numerical solution should show convergence to the physically correct entropy satisfying solution. Furthermore, the method should preserve mass locally and should be accurate up to second order in smooth regions of the solution.

The minmod slope limiter technique represents a method which has the required properties. Slope limiter methods for one-dimensional problems reduce slopes in the vicinity of discontinuities and belong, therefore, to the total variation diminishing (TVD) methods. The first TVD methods were introduced by van Leer [18]. There have been several developments made in the meantime by Engquist and Osher [13], Roe [19] and Sweby [20].

Slope limiting methods consist of three steps: first, in the one-dimensional case, a piecewise linear saturation distribution $\tilde{S}^n(x, t_n)$ using the given values $\{S_K^n\}$ from time level n is constructed. The minmod slope limiter belongs to the Φ-limiters ($1 \le \Phi \le 2$), whose slopes σ over each (one-dimensional) element are determined by

$$\sigma = \begin{cases} 1/2 \, (\text{sign}(\sigma_1) + \text{sign}(\sigma_2)) \max\{|\sigma_1|, |\sigma_2|\} & \sigma_1/\sigma_2 \le \Phi \wedge \sigma_2/\sigma_1 \le \Phi \\ \Phi 1/2 \, (\text{sign}(\sigma_1) + \text{sign}(\sigma_2)) \min\{|\sigma_1|, |\sigma_2|\} & \text{else} \end{cases}. \tag{56}$$

Equation (56), for the reconstruction of the saturation profile, is illustrated in Figure 3 for $\Phi = 1$ and $\Phi = 2$. This function is subsequently used to solve the conservation law (53) for the cell-average values $\{S_K^{n+1}\}$ of the saturation at time level $n+1$.

Minmod ($\Phi = 1$) is the Φ-limiter with the weakest CFL time step restriction and therefore a good choice for problems with non-linear fluxes. Some slope limiters, such as the minmod limiter, can be interpreted as flux limiters and vice versa [21].

The algorithm described so far corresponds to the Godunov flux [22], i.e. the mobilities are upstream weighted. However, problems are likely to occur at sonic points and stationary shocks. For this reason, the more sophisticated EO numerical flux developed by Engquist and Osher [13] is used. This adds diffusion to the system at critical points, in order to ensure stability and convergence to the entropy solution. Another alternative is the two-phase upstream weighted flux by Brenier and Jaffre [23]. In some cases, this flux scheme is more efficient.

In the two-dimensional case, the minmod slope limiter is again utilized for the bilinear reconstruction of the saturation distribution S_K in element K. Consequently, the solution of the saturation equation follows the same procedure as in the one-dimensional case. However, only average values of the edge saturations are needed, node values are not required. The resulting method represents a five-point scheme. In order to avoid grid orientation effects, a nine-point scheme is necessary. The minmod slope limiter method is in the one-dimensional case, total variation diminishing. However, in two dimensions, minmod has not this property anymore.

2.2.5. Global algorithm. The presented IMPES-based FE–FV method can be summarized by subdividing the solution of the mixed-hybrid formulation of the pressure equation into three procedures. First the mixed-hybrid system of equations is solved for the Lagrange multipliers $TP_{e_i}^{n+1}$. The element pressures P_K^{n+1} can then be obtained and the total fluxes $Q_{e_i}^{n+1}$ can be determined by Equation (45) using edge and element pressures. Then, when the pressure and velocity field of time level $n+1$ are known, the discretized saturation equation (52) is solved using the minmod limiter technique based on the EO numerical flux scheme.

3. COMPARISON OF THE TWO METHODS

The presented methods correspond to two completely different approaches for the solution of transient multiphase flow processes in heterogeneous porous media. The Galerkin-type finite

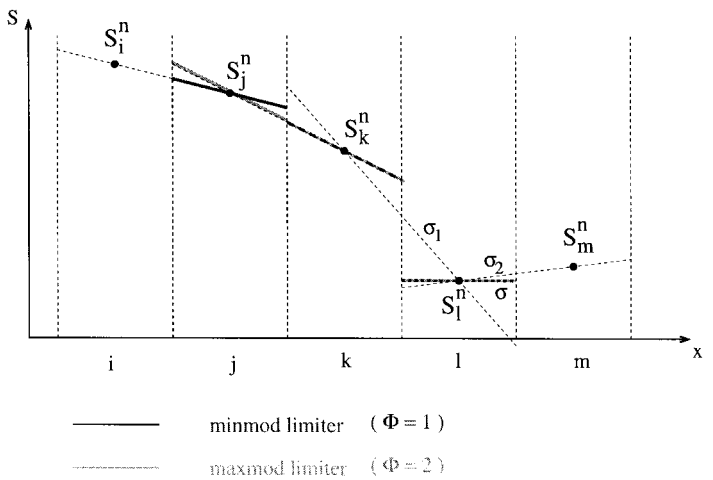

Figure 3. Piecewise linear reconstruction of the saturation by minmod ($\Phi = 1$) and maxmod ($\Phi = 2$) limiter.

element methods, such as the standard Galerkin, Petrov–Galerkin, and full-upwind Galerkin methods represent the classical approach to these problems [1,24]. For each phase, one differential equation is necessary. The primary variables, the pressure of one phase and the saturation of the other phase, are discretized by classical finite elements and consequently have continuous approximations. Physically, the saturation distribution is generally discontinuous. For instance, infiltration processes produce propagating shock fronts. Another example represent stationary jumps of the saturation which develop in the vicinity of sharp discontinuities of material properties.

In contrast to the node values of the Galerkin finite element approach, the numerical approximation of the pressure field by the mixed finite elements is represented by 'average values' over each element and edge of the discretized domain. The velocity field is described by the total fluxes over the element edges. These total fluxes guarantee that the method obeys a local mass conservation principle for each element. The pressure field is determined not only inside elements but, in the case of the mixed-hybrid method, on element edges. The Galerkin methods have node values for the pressure only. The classical FE solutions satisfy a global mass conservation principle only. Some classical finite element methods belong to the class of control-volume finite element methods and consequently conserve mass locally.

Although the same partition of the considered domain is used, boundary conditions, material properties such as absolute permeability, constitutive relationships, porosity, etc., are discretized in a different way. In contrast to the mixed finite element approach, the classical finite element discretization allows only continuous transitions of such quantities and properties. The mixed approach is characterized by discontinuous spatial representations of these material and fluid properties. Relative permeabilities are formulated on edges as well as inside of elements. For heterogeneous media, the absolute permeability tensor $\boldsymbol{K}$ should be harmonically weighted. This is done by the mixed-hybrid method in a natural way because it discretizes $\boldsymbol{K}^{-1}$ in Equation (45) [7]. In contrast to this, tensor $\boldsymbol{K}$ in the transmissivity integral (12) of the classical finite element methods must be substituted by its harmonical average of the corresponding node values. Both methods can easily be extended to compressible fluid flow. One advantage of the mixed finite element conception is that fluxes across element edges are unambiguous, even if an element edge constitutes an interface between regions of different material compositions and properties. This is not the case for classical finite elements. The velocities and fluxes are derived from the pressure gradients. However, at discontinuities in material and fluid properties, pressure gradients of different magnitude and orientation appear on each side of an element edge. This leads to ambiguous fluxes across element edges because the velocity field is determined by differentiation of the phase pressures.

The primary variables of the full-upwind Galerkin method are the pressure of one phase and the saturation of the other phase. They are solved simultaneously by an iterative scheme. This means that pressure and saturation have the same order of accuracy. The primary variables of the mixed finite element method are pressure and element edge fluxes. They are approximated simultaneously. One advantage of the mixed finite elements is that pressure and velocity fields have the same order of accuracy. In contrast, classical finite elements have velocities of an order less than the pressure approximation. This is because differentiation entails the loss of one order of accuracy. However, the advantage of a better approximation of fluxes and the ability to discretize saturations and material properties discontinuously is paid for by a decoupling of pressure and saturation inherent in the IMPES concept.

In addition to the ability to describe geometrically complex geological structures, the need to consider capillary pressure effects in highly heterogeneous soils becomes more and more important. Furthermore, the development and simulation of thermally enhanced remediation

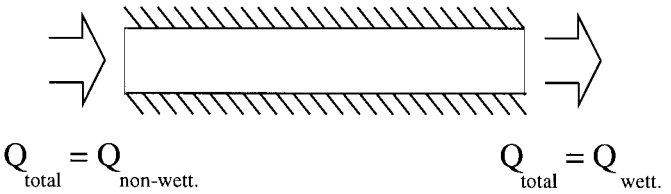

Figure 4. One-dimensional Buckley–Leverett problem.

techniques for contaminated soils requires the extension of three and more fluids to systems, and the inclusion of compressibility and non-isothermal effects on flow processes into the model. The aforementioned limitations underlying the IMPES method represent a problem when extending the method to systems of rapidly changing pressures and large capillary pressure effects.

Positive aspects of mixed methods are the short computation times for two-phase flow without capillary pressure effects, the high resolution of material heterogeneities and saturation fronts, and the better description of the posed initial boundary-value problems. However, one drawback of the method is the time step restrictions inherent in the explicit solution of the fluxes imposed by the CFL condition.

4. NUMERICAL EXAMPLES

The following numerical examples are non-dimensionalized so that physical units are avoided. In addition, the term 'PVI' for pore volumes injected is introduced.

4.1. One-dimensional problem in a homogeneous medium

First we will show the performance of the full-upwind Galerkin and the mixed-hybrid method with respect to flow in a homogeneous medium. The Buckley–Leverett problem [17] is a simple test problem without capillary pressure effects, where the quasi-analytical solution is easily derived [9,21]. It is excellent to investigate the two methods with respect to their convergence to the exact solution and their resolution of discontinuities. The Buckley–Leverett problem describes the displacement, in our case, of a wetting phase by a non-wetting phase from left to right where a constant total flux through the domain takes place (see Figure 4).

Initially, the total pore volume is filled with the wetting phase. A time independent boundary non-wetting phase saturation of one is assumed at the left end of the considered domain. The ratio of the fluid viscosities is one, and residual saturations are zero. For the relative permeability functions, the Brooks–Corey model is used with pore size distribution index $\lambda = 2.0$. The relative permeabilities then have the following form:

$$k_{\mathrm{rw}}(S_{\mathrm{w}}) = S_{\mathrm{w}}^4 \tag{57}$$

$$k_{\mathrm{rn}}(S_{\mathrm{w}}) = (1 - S_{\mathrm{w}})^2(1 - S_{\mathrm{w}}^2). \tag{58}$$

The one-dimensional domain is discretized by equidistant grids into 10, 20 and 40 elements with a time discretization of 20, 40 and 80 time steps, respectively.

Figure 5 shows the saturation profiles of the numerical methods and the quasi-analytical solution at 0.4 PVI, i.e. when 40% of the total pore volume is filled with the injected fluid. Both methods converge to the (quasi-) analytical solution. The full-upwind Galerkin finite

element method approaches the analytical solution in the smooth region, behind the shock front, from below. The mixed method approaches the analytical solution in smooth regions from above. In contrast to the Galerkin-type method which has too much numerical dispersion, the mixed finite element method shows a sharp resolution of the shock front, even for large discretization lengths.

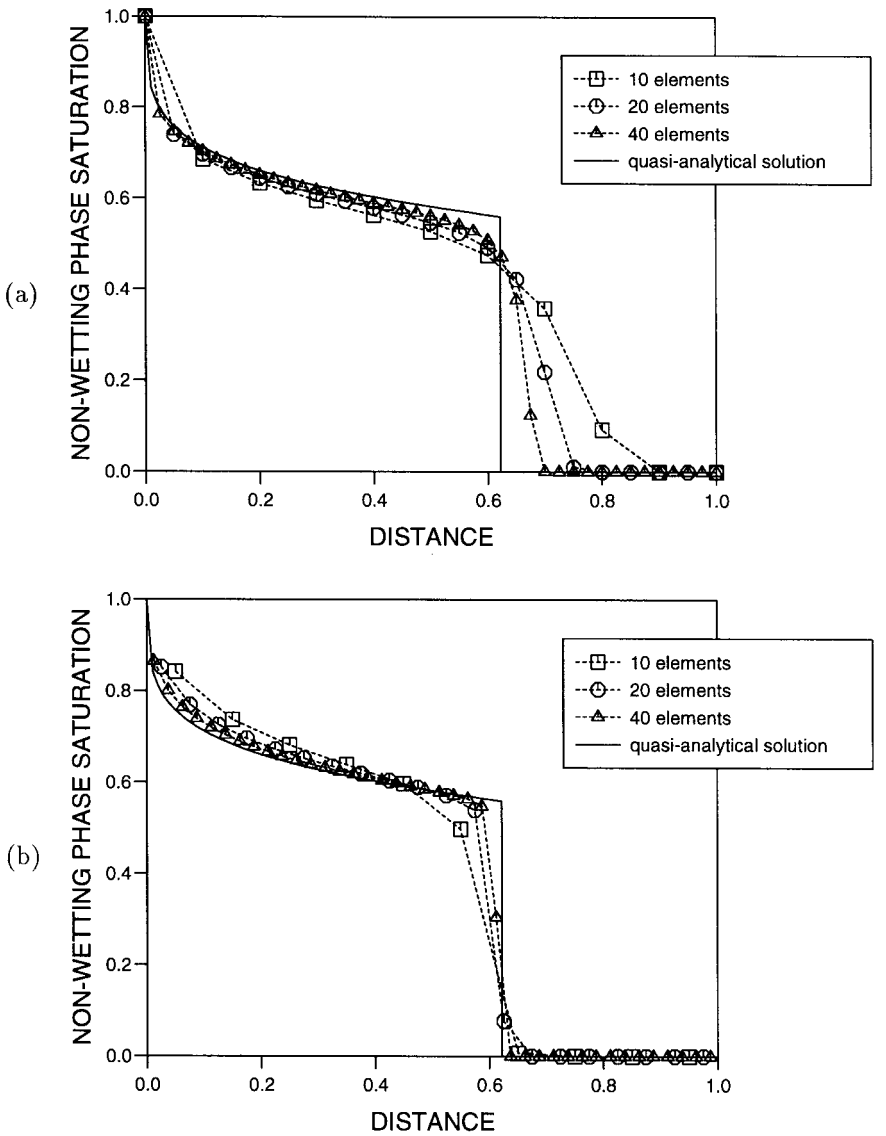

Figure 5. One-dimensional displacement of a wetting phase in a homogeneous porous medium at 0.4 PVI: (a) full-upwind Galerkin; (b) mixed-hybrid method.

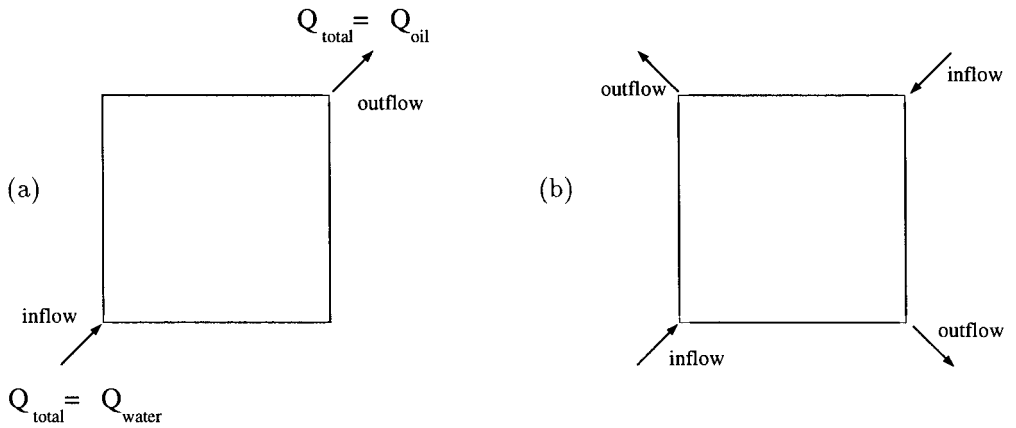

Figure 6. Five-spot waterflood problem: (a) diagonal grid; (b) parallel grid.

4.2. Five-spot waterflood problem

The five-spot waterflood problem described by Spivak *et al.* [25] comprises two cases. Analogously to the Buckley–Leverett problem, it deals with incompressible flow without capillary pressure effects—the displacement of oil by water within a square-shaped domain. Initially, there is no water present in the system. The square domain is discretized by regular grids of dimension 16×16, 32×32 and 64×64. The five-spot waterflood problem is a test case to investigate grid orientation effects of numerical schemes. In the first case, the 'diagonal grid' case, water is injected at the lower left corner and displaces the oil which flows out of the domain at the upper right corner (see Figure 6 (a)). The principal flow direction is diagonal to the grid.

The second case is similar to the first one but the water is now injected at the lower left corner and the upper right corner. The oil can leave the domain at the lower right corner and the upper left corner (see Figure 6 (b)). The main flow paths are parallel to the grid. For this reason, it is also called the 'parallel grid' case.

For both cases an 'ideal' numerical scheme should produce a quarter circle shaped saturation front of the injected water phase. Analogously to Spivak *et al.*, the relative permeability–saturation relationship after Todd is assumed.

It is given by

$$k_{\mathrm{rw}}(S_{\mathrm{w}}) = S_{\mathrm{w}}^2, \qquad k_{\mathrm{rn}}(S_{\mathrm{w}}) = (1 - S_{\mathrm{w}})^2, \tag{59}$$

and we assume a mobility ratio of $\mu_{\mathrm{n}}/\mu_{\mathrm{w}} = 4$. The fractional flow function is then

$$f_{\mathrm{w}}(S_{\mathrm{w}}) = \frac{4S_{\mathrm{w}}^2}{4S_{\mathrm{w}}^2 + (1 - S_{\mathrm{w}})^2}. \tag{60}$$

The initial condition is a uniform saturation of $S_{\mathrm{w}} = 0$ inside the domain. The results show the situation at 0.075 PVI for the diagonal grid case, and at 0.15 PVI in the case of the parallel grid. For the 16×16, 32×32 and 64×64 grids, the number of time steps used are 150, 300 and 600, respectively.

To get a better idea of how the numerical solutions converge to the exact solution, the cross-section of the water saturation profile along the diagonal line (x, y), $x = y$, for the diagonal grid case is shown in Figure 9. The 'exact' solution is computed from a fine-scale

finite difference solution of the radial Buckley–Leverett flow [26]. The radial Buckley–Leverett flow describes the situation where water is injected into the centre of a circular region. The corresponding differential equation is given by

$$\frac{\partial S_w}{\partial t} + \frac{1}{r}\frac{\partial}{\partial r}(rf(S_w, r)) = 0, \tag{61}$$

where r is the radial distance from the injection centre.

Because we are studying incompressible fluids, flux f has the form $f(S_w, r) = f_w(S_w)/r$, therefore, Equation (61) reduces to

$$\frac{\partial S_w}{\partial t} + \frac{1}{r}\frac{\partial f_w(S_w)}{\partial r} = 0, \tag{62}$$

and finally we obtain

$$\frac{\partial S_w}{\partial t} = -\frac{1}{r}\frac{\partial f_w(S_w)}{\partial S_w}\frac{\partial S_w}{\partial r}. \tag{63}$$

$\mathrm{d}f_w(S_w)/\mathrm{d}S_w$ is known for any value of S_w, and the remaining differential operators are discretized by backward finite differences.

Figure 7 shows that the full-upwind Galerkin method has no significant grid orientation effects (cross-diffusion). In contrast, for coarse grids, the mixed finite element method results in saturation profiles which are deformed quarter-circles. For both the diagonal and parallel grid cases, as depicted in Figure 8, the saturation fronts propagate faster along the boundaries of the square domain than in direction of the diagonal. With further grid refinement, these grid orientation effects suddenly vanish and the numerical solutions of the mixed method converge rapidly to the exact solution. This phenomenon is apparent when looking at the cross-sections of the saturation profiles of the diagonal grid case along the diagonal. While the curves of the full-upwind Galerkin method converge gradually, with much numerical dispersion and smearing, to the exact solution, the mixed finite element solutions show a rapid convergence from the 32×32 grid to the 64×64 grid. The grid orientation effects vanish rapidly when a certain level of refinement is reached.

4.3. Two-dimensional problem in a heterogeneous medium

The presented two-dimensional problem is analogous to the diagonal grid case of the five-spot waterflood problem. The domain corresponding to a reservoir or a part of the subsurface is a square with impermeable boundaries, except for an inflow and an outflow boundary at the lower left and upper right corner, respectively.

The non-wetting phase is injected into the domain at a constant flow rate. The same relative permeability–saturation relationships are used as in the former section. In contrast to the problem in this previous section, the absolute permeability is not constant over the considered domain. In the heterogeneous medium, a distribution of the absolute permeability of the form $\boldsymbol{K} = k\mathrm{Id}$ is assumed where k is log-normally distributed and Id is the identity matrix. The distribution (see Figure 9 and Figure 10(a)) is characterized by following parameters: $\log_{10}k$ has a mean of -5.0, a variance of 0.2, and a correlation length of 0.2. The discretization of the problem is carried out using a 32×32 regular grid and 600 time steps. The numerical results in Figure 10 (b)–(c) display the saturation distribution of the injected non-wetting phase at 0.3 PVI for the two methods. At the lower left corner, the injected non-wetting phase displaces the wetting-phase within the square domain. In high-permeable zones of the domain

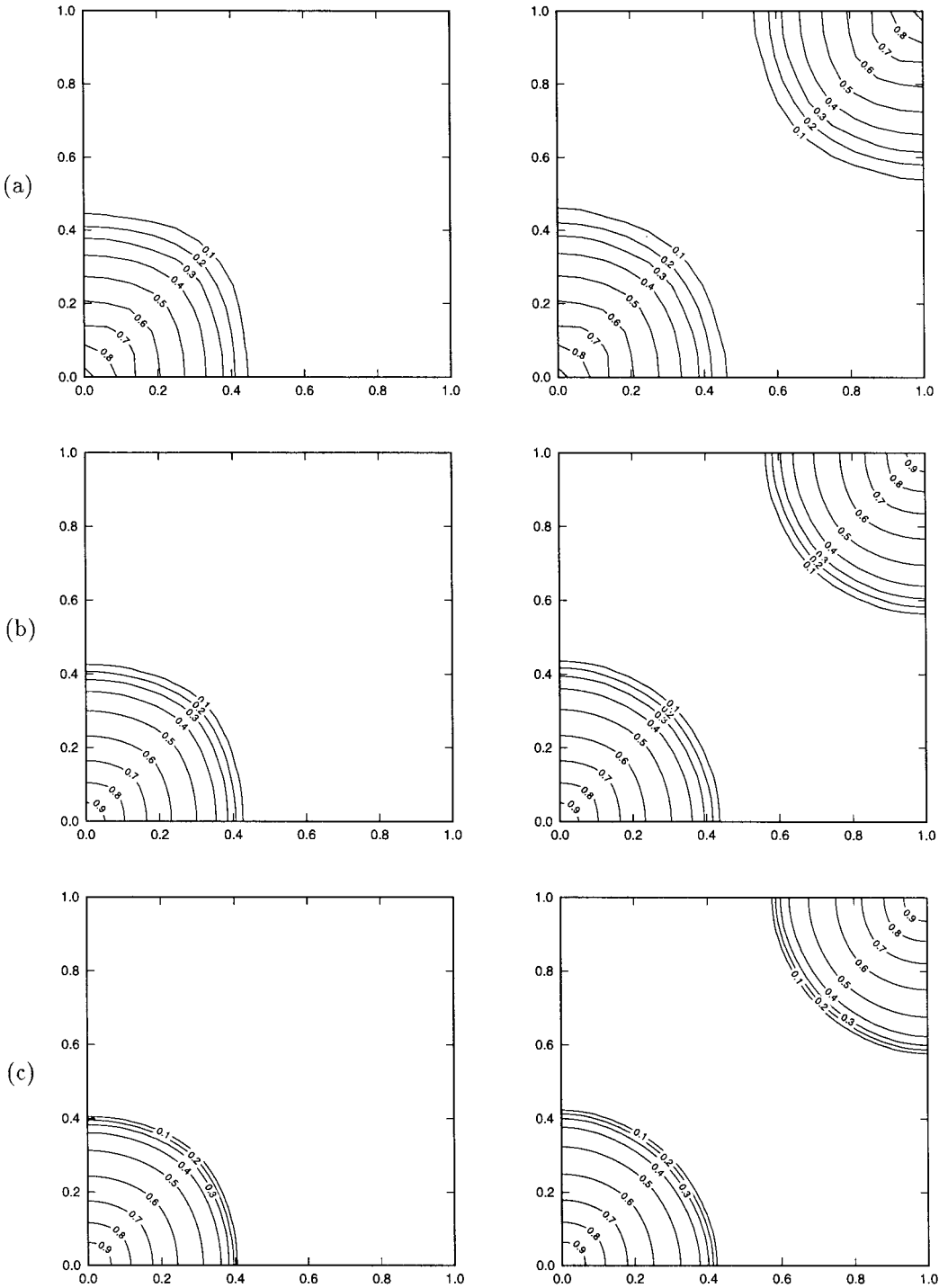

Figure 7. Numerical results of the full-upwind Galerkin method for the diagonal grid at 0.075 PVI (left), and for the parallel grid at 0.15 PVI (right): (a) 16×16; (b) 32×32; (c) 64×64 elements.

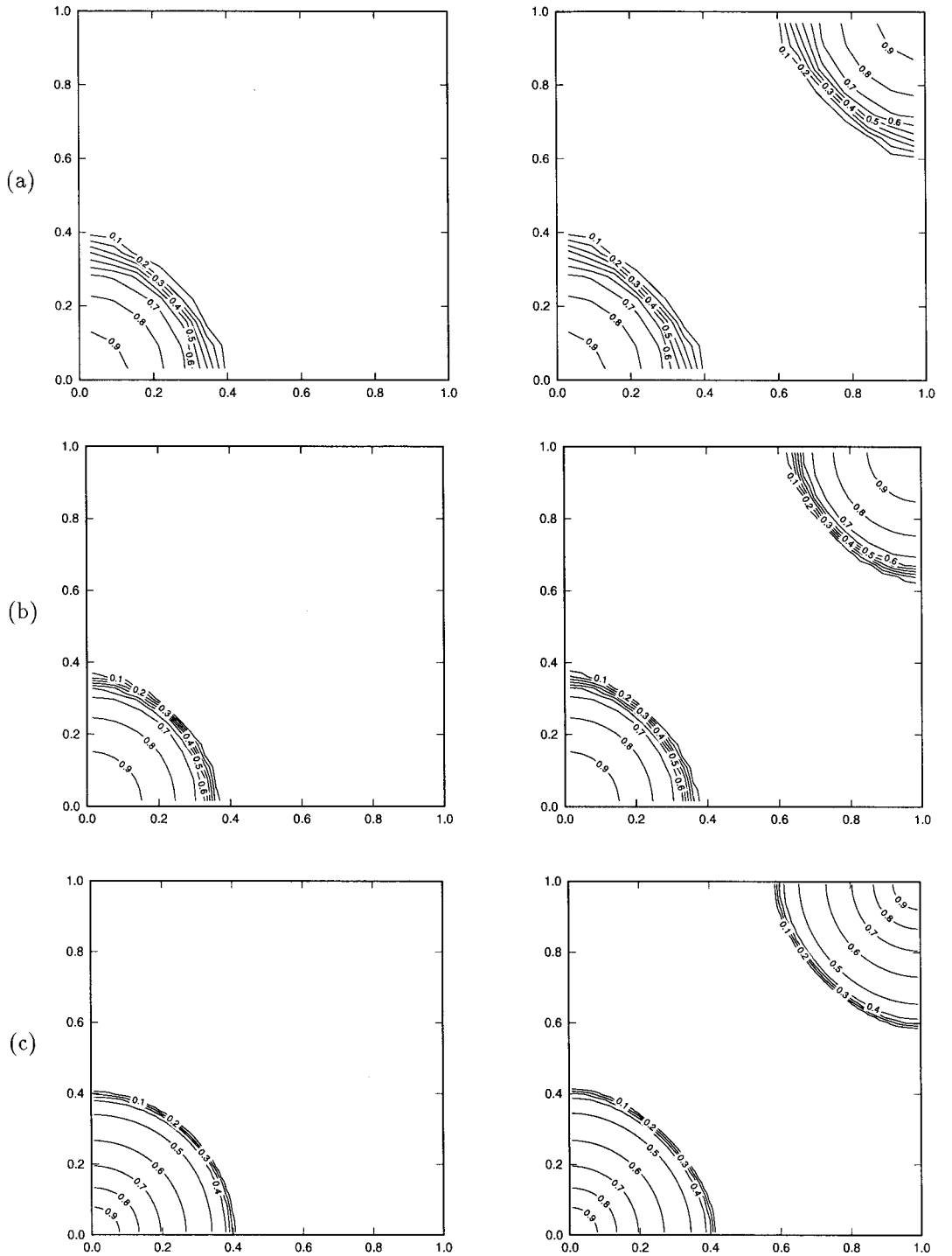

Figure 8. Numerical results of the mixed-hybrid method for the diagonal grid at 0.075 PVI (left), and for the parallel grid at 0.15 PVI (right): (a) 16×16; (b) 32×32; (c) 64×64 elements.

preferential flow paths develop, along which the displacing phase propagates faster. The numerical solution of the full-upwind Galerkin method shows a very smooth transition of the saturation. In contrast, the mixed method reveals a very sharp shock front. Because the same amount of non-wetting phase is injected, the saturation front of the full-upwind Galerkin method has propagated much further.

To give an idea of the computational savings the mixed-hybrid method provides for the calculation of the given problem compared with the full-upwind Galerkin method the sizes of the corresponding systems to be solved, and the computational effort are considered. The system matrix of the finite element method for a $n \times n$ element grid is of dimension $2(n+1)^2$,

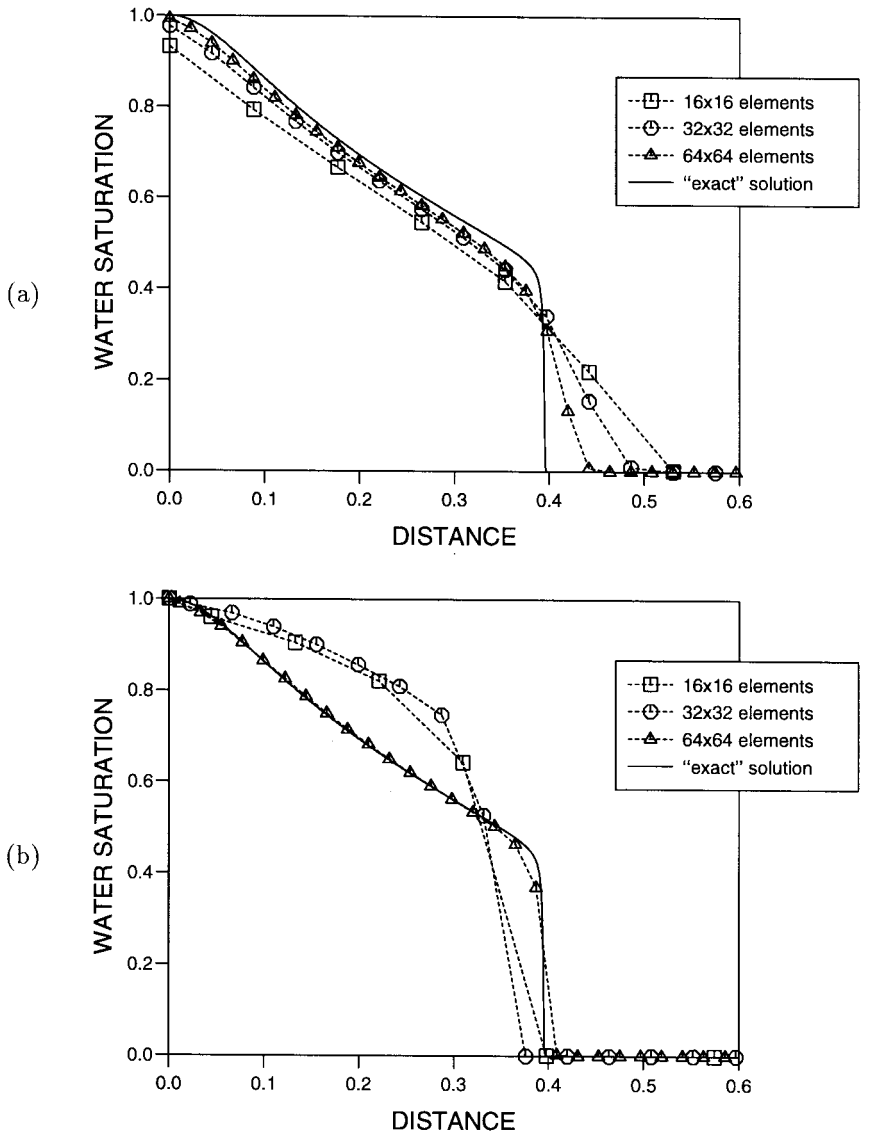

Figure 9. Five-spot waterflood problem (diagonal grid case): Cross-section of the water saturation profile along the diagonal line (x, y), $x = y$. (a) Full-upwind Galerkin; (b) mixed-hybrid method.

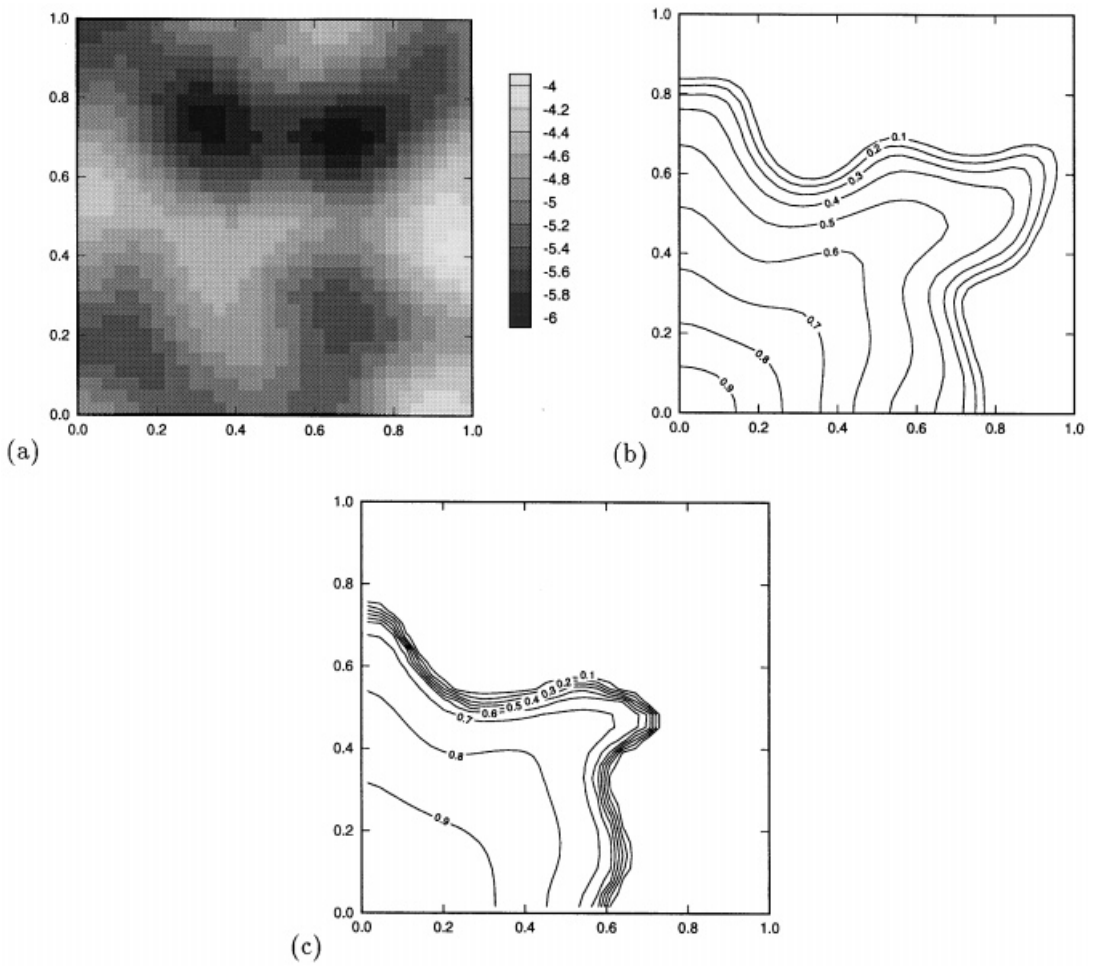

Figure 10. Flow in a heterogeneous medium: (a) permeability field ($\log_{10}k$); numerical results of the full-upwind Galerkin; and (b) the mixed-hybrid method; (c) at 0.3 PVI.

that is twice the number of nodes. The size of the corresponding mixed-hybrid system matrix is equal to the number of edges and amounts $2n(n+1)$. For both methods, the calculations were carried out on a HP 9000/C110 (HP-UX 10.10) machine. For the 600 time steps, the full-upwind Galerkin method takes 1216 Newton iterations with a total cpu time of 17725 s. Therefore, an average of 2.03 Newton steps are necessary per time step, with a computational effort of 14.58 s per Newton iteration.

For the given problem, the mixed-hybrid method is 13 times faster than the full-upwind Galerkin method (see Table I). This number gives an idea of the efficiency of the mixed-hybrid method for the simulation of convection–gravitation-dominated processes.

Table I. Computational effort

	Unit	Full-upwind Galerkin method	Mixed-hybrid method
Size of system matrix	—	2178	2112
Computation time per time step	s	29.54	2.26
Total computation time	s	17 725	1353

5. CONCLUSION

There are two main conceptions for future developments and extensions of existing codes and models for multiphase flow in heterogeneous porous media. One follows the control-volume finite element approach based on the coupled pressure–saturation equations, in conjunction with a Newton–Raphson iterative scheme. Mass is conserved locally over each control-volume. The iterative approach is well suited for the simulation of capillary pressure effects, e.g. the entry condition (bubbling pressure) [24]. It is easy to extend the given method to multi- (more than two) phase flow [1]. Moreover, this method can be modified for multi-phase compositional simulators [27], and physical aspects such as thermal influence [28], hysteresis, chemical reactions, etc. can easily be included into the scheme. Of course, the system can be formulated for three dimensions. One method which is based on the control-volume finite element approach is the presented full-upwind Galerkin method.

The decoupling of pressure and saturation of the IMPES philosophy is not suited to simulate processes where high changes of capillary pressure with respect to saturation occur, as it happens for diffusion-dominant processes. The employment of implicit flux limiting schemes is one option with which the problem may be dealt. However, any improvement regarding the approximation of the diffusive effects involves an additional computational effort [4]. On the other hand, if the changes of the pressure field with respect to the time are small and convective processes are dominant, then the IMPES method proves to be a much more efficient choice, as demonstrated in Section 4.3. For very slowly changing pressure fields, the pressure equation needs to be solved after several time steps, which saves a great deal of the computation time.

ACKNOWLEDGMENTS

Funding for the research described in this article was provided by Deutsche Forschungsge meinschaft, SFB 404 'Mehrfeldprobleme in der Kontinuumsmechanik'. The first author is supported by the foundation 'Besinnung und Ordnung'.

REFERENCES

1. R. Helmig, 'Theorie und numerik der mehrphasenströmungen in geklüftet-porösen medien', *Rep. 34*, *Inst. f. Strömungsmech. und Elektr. Rechnen im Bauwesen*, University of Hannover, 1993.
2. K. Pruess, *TOUGH 2, A General-Purpose Numerical Simulator for Multiphase Fluid and Heat Flow*, LBL, University of California, Berkeley, 1991.
3. P.A. Forsyth, 'A control volume finite element approach to NAPL groundwater contamination', *SIAM J. Sci. Stat. Comp.*, **12**, 1029–1057 (1991).
4. G. Chavent and J. Jaffre, 'Mathematical models and finite elements for reservoir simulation', North Holland, Amsterdam, 1986.
5. G. Chavent and J.E. Roberts, 'A unified physical presentation of mixed, mixed-hybrid finite elements and standard finite difference approximations for the determination of velocities in waterflow problems', *Adv. Water Res.*, **14**, 329–348 (1991).

6. L.J. Durlofsky, 'A triangle based mixed finite element–finite volume technique for modelling two phase flow through porous media', *J. Comp. Phys.*, **105** 252–266 (1993).
7. L.J. Durlofsky, 'Accuracy of mixed and control volume finite element approximations to Darcy velocity and related quantities', *Water Resources Res.*, **30**, 965–973 (1994).
8. R. Helmig, 'Coupled flow and transport processes in the subsurface', *Environm. Eng.*, Springer, Berlin (to appear).
9. R. Huber, 'Kopplung von FE-/FV-methoden zur numerischen simulation von zweiphasenströmungen in heterogenen, porösen Medien', *M.Sc. Thesis*, University of Stuttgart, 1995.
10. R. Helmig, M. Emmert and H. Sheta, 'Modelling of multiphase flow in heterogeneous porous media and applications', *Proc. 6th Int. Conf. Comput. in Civil and Building Eng.*, Berlin, 1995.
11. R. Helmig, M. Emmert and H. Sheta, 'Problems and issues of constitutive relationships needed for accurate modelling of multiphase flow in heterogeneous porous media', in *Groundwater and Subsurface Remediation, Environm. Eng.*, Springer, Berlin, 1996, pp. 245–264.
12. D.W. Peaceman, *Fundamentals of Numerical Reservoir Simulation*, Elsevier, Amsterdam, 1977.
13. B. Engquist and S. Osher, 'One-sided difference approximations for nonlinear conservation laws', *Math. Comp.*, **36**, 321–351 (1981).
14. F. Brezzi and M. Fortin, 'Mixed and hybrid finite element methods', *Springer Series in Comput. Mathematics*, **15** (1991).
15. P.A. Raviart and J.M. Thomas, 'A mixed finite element method for 2nd order elliptic problems', in *Mathematical Aspects of the Finite Element Method, Lecture Notes in Mathematics*, Vol. 606, Springer, Berlin, 1977, pp. 292–315.
16. C.W. Shu and S. Osher, 'Efficient implementation of essentially non-oscillatory shock-capturing schemes', *J. Comp. Phys.*, **77** 439–471 (1988).
17. S.E. Buckley and M.C. Leverett, 'Mechanism of fluid displacements in sands', *TAIME*, **146**, 107–116 (1942).
18. B. van Leer, 'Towards the ultimate conservative difference scheme I. The quest of monotonicity', in *Springer Lecture Notes in Physics*, **18**, 163–168 (1973).
19. P.L. Roe, 'Approximate Riemann solvers, parameter vectors, and difference schemes', *J. Comp. Phys.*, **43**, 357–372 (1981).
20. P.K. Sweby, 'High resolution schemes using flux limiters for hyperbolic conservation laws', *SIAM J. Numer. Anal.*, **21** 995–1011 (1984).
21. R.J. LeVeque, 'Numerical methods for conservation laws', in *Lectures in Mathematics*, ETH Zürich, Birkhäuser, Basel, 1992.
22. S.K. Godunov, 'A finite difference method for the numerical computation of discontinuous solution of the equation of flow dynamics', *Mat. Sb.*, **47**, 271–290 (1959).
23. Y. Brenier and J. Jaffre, 'Upstream differencing for multiphase flow in reservoir simulation, *SIAM J. Numer. Anal.*, **28**, 685–696 (1991).
24. R. Helmig and R. Huber, 'Comparison of different Galerkin-type discretization techniques for two-phase flow in heterogeneous porous media', *Rep. 96/11, Sonderforschungsbereich 404*, University of Stuttgart, 1996.
25. A. Spivak, H.S. Price and A. Settari, 'Solution of the equations for multidimensional, two-phase, immiscible flow by variational methods', *SPE J.*, **2**, 27–41 (1977).
26. M. Blunt and B. Rubin, 'Implicit flux limiting schemes for petroleum reservoir simulation', *J. Comp. Phys.*, **102**, 194–210 (1992).
27. A.J.A. Unger, P.A. Forsyth and E.A. Sudicky, 'Variable spatial and temporal weighting schemes for use in multi-phase compositional problems', *Adv. Water Res.*, **19**, 1–27 (1996).
28. M. Emmert, 'Numerische modellierung nichtisothermer gas–wasser systeme in porösen medien', *Ph.D. Thesis*, University of Stuttgart, 1996.

